APL Materials

Elastic modulus and coefficient of thermal expansion of piezoelectric $Al_{1-x}Sc_xN$ (up to x = 0.41) thin films

Cite as: APL Mater. **6**, 076105 (2018); https://doi.org/10.1063/1.5040190
Submitted: 15 May 2018 • Accepted: 12 July 2018 • Published Online: 26 July 2018

Yuan Lu, Markus Reusch, Nicolas Kurz, et al.

open access

View Online Export Citation CrossMark

ARTICLES YOU MAY BE INTERESTED IN

AlScN: A III-V semiconductor based ferroelectric
Journal of Applied Physics **125**, 114103 (2019); https://doi.org/10.1063/1.5084945

Experimental determination of the electro-acoustic properties of thin film AlScN using surface acoustic wave resonators
Journal of Applied Physics **126**, 075106 (2019); https://doi.org/10.1063/1.5094611

Optical constants and band gap of wurtzite $Al_{1-x}Sc_xN/Al_2O_3$ prepared by magnetron sputter epitaxy for scandium concentrations up to x = 0.41
Journal of Applied Physics **126**, 045715 (2019); https://doi.org/10.1063/1.5101043

AMERICAN ELEMENTS
THE ADVANCED MATERIALS MANUFACTURER
The Next Generation of Material Science Catalogs
Now Invent.™
www.americanelements.com

AIP Publishing

© 2018 Author(s).

APL MATERIALS **6**, 076105 (2018)

Elastic modulus and coefficient of thermal expansion of piezoelectric $Al_{1-x}Sc_xN$ (up to x = 0.41) thin films

Yuan Lu,[1] Markus Reusch,[1] Nicolas Kurz,[2] Anli Ding,[1] Tim Christoph,[1] Mario Prescher,[1] Lutz Kirste,[1] Oliver Ambacher,[1,3] and Agnė Žukauskaitė[1]
[1]*Fraunhofer Institute for Applied Solid State Physics IAF, Tullastraße 72, 79108 Freiburg, Germany*
[2]*Laboratory for Compound Semiconductor Microsystems, IMTEK—Department of Microsystems Engineering, University of Freiburg, Georges-Koehler-Allee 103, 79110 Freiburg, Germany*
[3]*Laboratory for Power Electronics, INATECH-Deportment of Sustainable System Engineering, Emmy-Norther-Straße 2, 79110 Freiburg, Germany*

(Received 15 May 2018; accepted 12 July 2018; published online 26 July 2018)

Aluminum scandium nitride ($Al_{1-x}Sc_xN$ with x = 0–0.41) thin films were deposited by reactive pulsed-DC magnetron sputtering on Si(001) and Al_2O_3(0001) substrates. X-ray diffraction indicated high degree of c-axis orientation in all the films, and based on pole figure measurements, epitaxial relationship could be defined as $[10\bar{1}0]_{AlScN}//[11\bar{2}0]_{sapphire}$ and $(0001)_{AlScN}//(0001)_{sapphire}$ in films deposited on Al_2O_3. Piezoelectric coefficient increased up to d_{33} = 31.6 pC/N in $Al_{0.59}Sc_{0.41}N$, which is 550% higher than for AlN. The biaxial elastic modulus and the in-plane coefficient of thermal expansion (CTE) as a function of Sc concentration were determined by thermal cycling method: biaxial elastic modulus decreased from 535 GPa in pure AlN to 269 GPa in $Al_{0.59}Sc_{0.41}N$ and CTE was 4.65×10^{-6} K^{-1} for AlN and 4.29×10^{-6} K^{-1} for $Al_{0.59}Sc_{0.41}N$. Additionally, we observed an increase in CTE from 4.18×10^{-6} K^{-1} at 65 °C to up to 6.38×10^{-6} K^{-1} at 375 °C for $Al_{0.68}Sc_{0.32}N$. The experimentally determined CTE and elastic modulus allow a more precise design of $Al_{1-x}Sc_xN$-based frequency filters which are used in mobile communications and are important parameters for the prediction of device performance at elevated temperatures. © *2018 Author(s). All article content, except where otherwise noted, is licensed under a Creative Commons Attribution (CC BY) license (http://creativecommons.org/licenses/by/4.0/).* https://doi.org/10.1063/1.5040190

$Al_{1-x}Sc_xN$ has drawn a lot of attention as an attractive material for radio frequency microelectromechanical systems (RF-MEMS) after the discovery of its enhanced piezoelectric coefficient d_{33} = 27.6 pC/N for x = 0.43 compared with 6 pC/N for pure AlN[1] and increased electromechanical coupling k_t^2 from 7% in AlN to 15% in $Al_{0.7}Sc_{0.3}N$.[2] For MEMS device design, the mechanical properties, such as elastic modulus, and the coefficient of the thermal expansion (CTE) are important parameters.[3] However, there are only a few publications that experimentally assess the elastic properties of this novel material and there is only one report on the elastic modulus of $Al_{1-x}Sc_xN$ with relatively high Sc concentration.[4] Moreover, to the best of our knowledge, the CTE of $Al_{1-x}Sc_xN$ thin films has not been reported until now, and in addition to providing support for device design, it is also a significant parameter for the accurate determination of the pyroelectric coefficient of $Al_{1-x}Sc_xN$.[5]

As reported in the literature, elastic modulus of $Al_{1-x}Sc_xN$ thin films can be locally measured by nanoindentation.[3,6] However, the indentation modulus can be influenced by the indentation depth, the substrate, and other factors.[7] Measuring the temperature-stress relationship of thin films grown on substrates with different CTE is a non-destructive method that enables the determination of not only the elastic modulus but the CTE as well, as it was previously reported for AlN[8] and other materials.[9,10] The temperature-induced stress σ_T can be described by the following equation:[11]

 © Author(s) 2018

$$\sigma_T = \frac{E_f}{\left(1 - \upsilon_f\right)} \int_{T_2}^{T_1} (\alpha_s - \alpha_f) dT, \quad (1)$$

where $E_f/(1-\nu_f)$ is the biaxial elastic modulus and E_f and ν_f are Young's modulus and Poisson ratio of the film, respectively. α_s and α_f stand for the CTE of the substrate and the film, respectively. The CTE of the film α_f can also be described by the following:

$$\alpha_f = \frac{\alpha_{s1} - k\alpha_{s2}}{1 - k}, \quad (2)$$

where $k = (\Delta\sigma_{s1}/\Delta T)/(\Delta\sigma_{s2}/\Delta T)$ is the ratio of stress-temperature slopes, which is calculated based on temperature-induced stress as a function of temperature on substrates "s1" with CTE α_{s1} and "s2" with CTE α_{s2}.

In this work, we extracted the CTE and biaxial elastic modulus of $Al_{1-x}Sc_xN$ based on (1) and (2) by analyzing thin films deposited on Ø = 100 mm Si(001) and Al_2O_3(0001) substrates. 1 μm $Al_{1-x}Sc_xN$ (x = 0–0.41) thin films were grown by reactive pulsed-DC magnetron sputtering (Evatec Radiance) in pure N_2 reactive atmosphere from 100 mm Al (99.995% pure) and Sc (99.99% pure) targets. The Sc concentration in $Al_{1-x}Sc_xN$ was tuned by keeping the total magnetron power $P_{Al} + P_{Sc}$ constant at 1000 W while adjusting the individual magnetron powers. More details about the growth process can be found elsewhere.[12] The sputtering parameters are shown in Table I.

$Al_{1-x}Sc_xN/Al_2O_3$ thin films have higher tensile stress compared with $Al_{1-x}Sc_xN$/Si with corresponding Sc concentration due to lattice mismatch. In order to avoid cracks in $Al_{1-x}Sc_xN/Al_2O_3$, the heater temperature was decreased to 400 °C, while 500 °C was used for $Al_{1-x}Sc_xN$/Si to achieve higher crystalline quality. Scanning electron microscope (Zeiss Auriga Crossbeam FIB-SEM) with energy dispersive X-ray (EDX) spectroscopy (Bruker Quantax) was used to determine the film composition; the uncertainty with EDX is in the range of x ± 0.02 in $Al_{1-x}Sc_xN$.

To investigate the crystallinity of the $Al_{1-x}Sc_xN$(0001) thin films, X-ray diffraction (XRD) $2\theta/\theta$ scans and $Al_{1-x}Sc_xN$ 0002 reflection rocking curves (ω-scans) were recorded by PANalytical X'Pert Pro MRD diffractometer equipped with Ge 220 hybrid monochromator providing Cu-Kα_1 radiation. All of the $Al_{1-x}Sc_xN$ thin films on both Si(001) and Al_2O_3(0001) substrates showed only 000*l* (l = 2, 4, 6) reflections in $2\theta/\theta$ scans, indicating c-axis-oriented growth [Figs. 1(a) and 1(b)]. Texture analysis (XRD pole figure measurements) was done at wurtzite-type AlN $10\bar{1}1$ reflection position [insets in Figs. 1(a) and 1(b)]. For all $Al_{1-x}Sc_xN$/Si samples, a closed ring is seen at the polar angle $\psi = 62°$, which indicates fiber textured material with no preferential orientation in-plane,[8,13] and for $Al_{1-x}Sc_xN/Al_2O_3$, the 6-fold symmetry was observed with the rotation of 30° between the substrate and the film, typical of epitaxial growth of group-III nitrides on Al_2O_3 substrates,[14,15] where the epitaxial relationship can be defined as $[10\bar{1}0]_{AlScN}//[11\bar{2}0]_{sapphire}$ and $(0001)_{AlScN}//(0001)_{sapphire}$. Peak shift of $Al_{1-x}Sc_xN$ 0002 is due to different texture on Si and Al_2O_3 substrates, thermal strain caused by heater temperature during the deposition, as well as Sc concentration. It is reported that higher Sc concentration may lead to a peak shift toward lower[16,17] or higher 2θ angles.[18,19] The full width at half maximum (FWHM) of $Al_{1-x}Sc_xN$ 0002 reflection rocking curves was determined by fitting of pseudo-Voigt function [Fig. 2(a)]. In the $Al_{1-x}Sc_xN$/Si, with increasing Sc concentration, the FWHM is decreasing from 1.9° for AlN to 1.4° for $Al_{0.59}Sc_{0.41}N$, indicating improved film quality. Based on theoretical predictions, the mixing enthalpy in $Al_{1-x}Sc_xN$ is increasing with increasing Sc concentration and should lead to degradation in crystallinity.[20] However, in similar studies of sputtered $Al_{1-x}Sc_xN$/Si, no significant correlation between 0002 reflection rocking curve FWHM and

TABLE I. Sputtering parameters for $Al_{1-x}Sc_xN$ on Si(001) and Al_2O_3(0001).

Parameter	Value
$P_{Al} + P_{Sc}$	1000 W
Sc concentration x	0 (AlN), 0.06, 0.14, 0.23, 0.32, and 0.41
Process pressure	$<1.5 \times 10^{-1}$ Pa
N_2 gas flow	20 SCCM
Target-to-substrate distance	65 mm
Heater temperature	400 °C (Al_2O_3), 500 °C (Si)

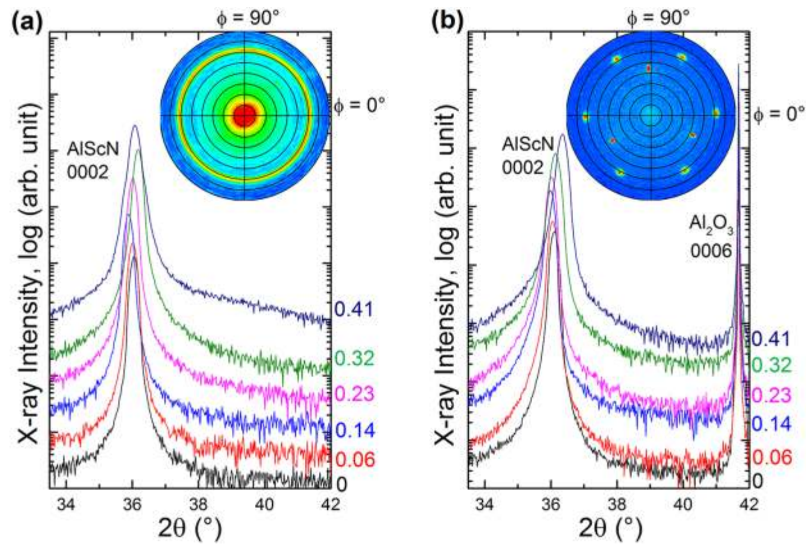

FIG. 1. (a) X-ray diffraction $2\theta/\theta$ scans for $Al_{1-x}Sc_xN/Si$ with x = 0–0.41 and pole figure of $Al_{0.68}Sc_{0.32}N/Si$ (inset); (b) X-ray diffraction $2\theta/\theta$ scans for $Al_{1-x}Sc_xN/Al_2O_3$ with x = 0–0.41 and pole figure $Al_{0.68}Sc_{0.32}N/Al_2O_3$ (inset). This figure will appear in color online.

Sc concentration was observed.[18] In the $Al_{1-x}Sc_xN/Al_2O_3$, the FWHM increases from 0.7° for AlN to 1.6° for $Al_{0.59}Sc_{0.41}N$, indicating marginal degradation of the film quality in the $Al_{1-x}Sc_xN/Al_2O_3$ for high Sc concentrations.

The clamped piezoelectric coefficient $d_{33,\text{clamp}}$ of $Al_{1-x}Sc_xN/Si$ was measured by Berlincourt method (Piezotest PM300) on diced 1 × 1 cm^2 samples with sputtered Ti electrodes,[12] and d_{33} corrected for influence of substrate stiffness[21] was calculated based on the following equation:[21]

$$d_{33} = d_{33,clamp} + 2d_{31}(S_{13} + \sigma/Y)/(S_{11} + S_{12}), \tag{3}$$

where the σ and Y are the Poisson ratio and Young's modulus of Si,[22] respectively, and theoretical values for d_{31}, S_{11}, and S_{12} for $Al_{1-x}Sc_xN$ are based on literature.[4] The corrected d_{33} increases from 5.5 pC/N for pure AlN to 31.6 pC/N for $Al_{0.59}Sc_{0.41}N$ [Fig. 2(b)] and concurs well with theoretical predictions,[4] as well as is comparable with the published values by Akiyama *et al.*,[1] confirming the high quality of the material.

To determine the film stress in as-deposited $Al_{1-x}Sc_xN$, first the film thickness was measured by ellipsometry (SENTECH SE800), the wafer curvature before and after the sputtering was measured by

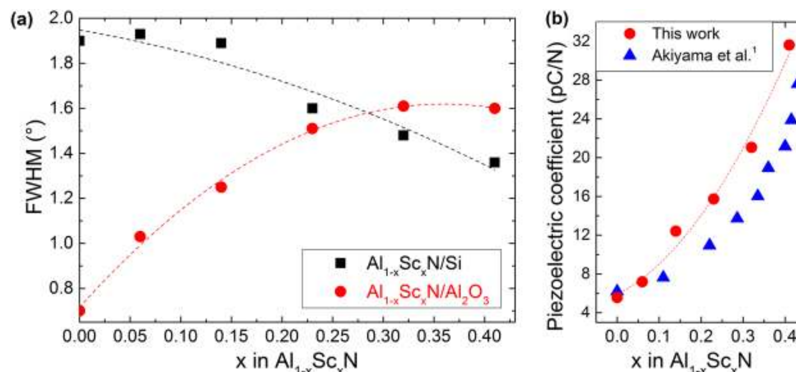

FIG. 2. (a) Rocking curve FWHM of AlScN 0002 reflection rocking curves as a function of the Sc concentration in $Al_{1-x}Sc_xN/Si$ (black squares) and $Al_{1-x}Sc_xN/Al_2O_3$ (red circles); (b) Piezoelectric coefficient d_{33} as a function of the Sc concentration. Lines are a guide for the eye.

FSM 500TC laser profiler, and then the in-plane stress σ was calculated by using Stoney-equation,[23]

$$\sigma = \frac{E_s d_s^2}{6(1 - \upsilon_s) d_f}\left(\frac{1}{R} - \frac{1}{R_0}\right), \tag{4}$$

where the $E_s/(1 - \nu_s)$ is biaxial elastic modulus of the substrate and d_f and d_s are the thicknesses of the film and the substrate, respectively. R_0 and R stand for the radius of curvature before and after the film deposition. In order to determine the CTE and the biaxial elastic modulus of $Al_{1-x}Sc_xN$, the temperature-induced stress was measured under N_2 atmosphere, in the same laser profiler experimental setup. First, thermal cycling for $Al_{1-x}Sc_xN/Si$ and $Al_{1-x}Sc_xN/Al_2O_3$ samples was done between room temperature and 400 °C with heating and cooling rate of 2 K/min, where every 25 K the temperature was held constant for 5 min before the wafer curvature measurement was performed. However, $Al_{1-x}Sc_xN/Al_2O_3$ samples with x = 0.06 and 0.14 were prone to cracking at elevated temperatures, and thus, the maximum temperature in the thermal cycling experiments was reduced to 125 °C with 2 K/min heating and cooling rate and the wafer curvature was recorded every 10 K for improved accuracy [Fig. 3(a), red circles].

Additional thermal cycling experiments under the same conditions were also performed for $Al_{1-x}Sc_xN/Si$ samples, and the stress-temperature slopes did not show any significant difference from the original thermal cycling series up to 400 °C; thus, the original measurement data were used. To investigate the possible film quality degradation or structural changes before and after the thermal cycling, FWHM of $Al_{1-x}Sc_xN$ 0002 reflection rocking curve was compared, showing ±0.1° difference for all the investigated samples; sample composition recorded in SEM-EDX varied only within the measurement error; surface roughness R_{rms} < 1.5 nm was measured by atomic force microscopy both before and after the thermal cycling, indicating that the samples did not undergo any irreversible changes in their microstructural or crystalline properties.

For calculation of the $Al_{1-x}Sc_xN$ CTE and biaxial elastic modulus, we first assume the constant CTE in the temperature range of 25-400 °C, and the following literature values are used for Si(001): biaxial elastic modulus $E_s/(1 - \nu_s)$ = 180 GPa[22] and CTE $\alpha = 3.57 \times 10^{-6}$ K^{-1},[24] and for Al_2O_3(0001):[25] biaxial elastic modulus $E_s/(1 - \nu_s)$ = 472.6 GPa and CTE $\alpha = 5.23 \times 10^{-6}$ K^{-1}.

Due to the different substrate CTE, the $Al_{1-x}Sc_xN/Si$ films become more compressive stressed and the $Al_{1-x}Sc_xN/Al_2O_3$ become more tensile; as an example, the temperature-induced stress curves recorded for $Al_{0.94}Sc_{0.06}N$ are shown in Fig. 3(a). Using (1) and (2), the average CTE and the biaxial elastic modulus were calculated and the results are shown in Fig. 3(b); here, the error originates from scattering of the data when fitting the stress-temperature slope and increases with the Sc concentration. Based on our measurements, CTE of AlN was determined to be $\alpha = 4.65 \pm 0.20 \times 10^{-6}$ K^{-1} (black squares), while values in the literature range from 2.56 to 5.27 × 10^{-6} K^{-1} [5,26,27] and biaxial elastic modulus of 535 GPa (blue circles) while 450-489 GPa has been reported previously.[4,8] With increasing Sc concentration, the CTE of $Al_{1-x}Sc_xN$ first increases and reaches the highest value of $\alpha = 4.95 \pm 0.26 \times 10^{-6}$ K^{-1} at x = 0.23 and then decreases down to $\alpha = 4.29 \pm 0.36 \times 10^{-6}$ K^{-1} for x = 0.41. The biaxial elastic modulus of $Al_{1-x}Sc_xN$ as a function of Sc decreases linearly by

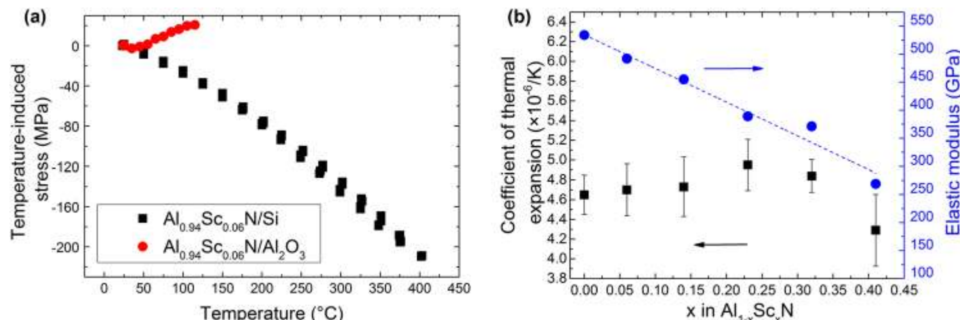

FIG. 3. (a) Temperature-induced stress as a function of temperature in $Al_{0.94}Sc_{0.04}N$ grown on Si(001) (black squares) and on Al_2O_3 (0001) (red circles); (b) Biaxial elastic modulus (blue circles) and average coefficient of thermal expansion (black squares) as a function of Sc concentration in $Al_{1-x}Sc_xN$. Lines are a guide for the eye.

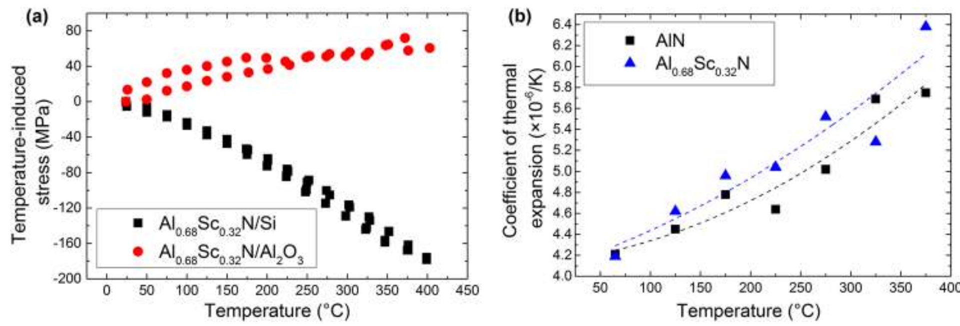

FIG. 4. (a) Temperature-induced stress as a function of temperature in $Al_{0.68}Sc_{0.32}N$ grown on Si(001) (black squares) and on Al_2O_3 (0001) (red circles); (b) Temperature-dependent coefficient of thermal expansion of AlN (black squares) and $Al_{0.68}Sc_{0.32}N$ (blue triangles) as a function of temperature. Lines are a guide for the eye.

$E_f/(1-v_f) = 534.77 - x{\cdot}601.36$ GPa. Our findings are in good agreement with theoretically predicted and experimentally determined biaxial elastic modulus by Caro *et al.*[4] The non-linear behavior of CTE could be explained by the non-linear evolution of lattice parameter *c*,[1,20,28] suggesting that the shape of the unit cell is changing non-linearly as a function of Sc concentration. However, in-depth theoretical study needed to explain this behavior is outside the scope of the current work.

In addition, the temperature-dependent CTE of AlN and $Al_{0.68}Sc_{0.32}N$ was calculated by using temperature-dependent stress data [Fig. 4(a)] as well as temperature-dependent Si(001) and Al_2O_3(0001) CTE every 50 °C.[24,25] The calculation of temperature-dependent CTE helps not only in the optimization of the mechanical properties during film deposition but also in the design of the temperature-compensated devices.[29,30] Figure 4(b) shows the CTE of AlN (black squares) and $Al_{0.68}Sc_{0.32}N$ (blue triangles) as a function of temperature. The CTE increases with temperature from 4.21×10^{-6} K^{-1} at 65 °C to 5.75×10^{-6} K^{-1} at 400 °C for AlN and from 4.18×10^{-6} K^{-1} at 65 °C to 6.38×10^{-6} K^{-1} at 400 °C for $Al_{0.68}Sc_{0.32}N$. Similar trends in literature can be seen in previous studies of temperature-dependent CTE in AlN.[24,31] Summary of experimentally determined average CTE and elastic modulus as a function of Sc concentration as well as calculated values based on literature are summarized in Table II.

In conclusion, growth of highly c-axis-oriented thin films of $Al_{1-x}Sc_xN$ with up to Sc concentration x = 0.41 on Si(001) and Al_2O_3(0001) substrates was achieved by pulsed-DC magnetron sputtering. Epitaxial relationship $[10\bar{1}0]_{AlScN}//[11\bar{2}0]_{sapphire}$ and $(0001)_{AlScN}//(0001)_{sapphire}$ was determined for all $Al_{1-x}Sc_xN/Al_2O_3$ samples. Rocking curve FWHM of AlScN 0002 reflection was $<2°$ for all the investigated samples, indicating a high crystalline quality suitable for device fabrication, as also confirmed by 550% higher d_{33} measured in $Al_{0.59}Sc_{0.41}N$/Si as compared with that in AlN. The in-plane CTE and the biaxial elastic modulus of AlN and $Al_{1-x}Sc_xN$ were simultaneously determined by the thermal cycling method. The CTE of AlN was in the same range as typical literature values, and this is the first report of CTE of $Al_{1-x}Sc_xN$ as a function of Sc concentration. The biaxial modulus is decreasing linearly to 270 GPa in $Al_{0.59}Sc_{0.41}N$ compared with 535 GPa in AlN, matching the theoretical predictions. Interestingly, the CTE was non-linear and was highest at x = 0.23, while later decreasing again, which could be caused by anisotropic evolution of the out-of-plane lattice

TABLE II. Experimental CTE, elastic modulus, and theoretical elastic modulus of $Al_{1-x}Sc_xN$.

Sc concentration x	CTE ($\times10^{-6}$ K^{-1})	Elastic modulus (GPa)	Elastic modulus in literature[a] (GPa)
0 (AlN)	4.65 ± 0.20	535	490
0.06	4.70 ± 0.26	492	452
0.14	4.73 ± 0.30	456	415
0.23	4.95 ± 0.26	389	367
0.32	4.84 ± 0.17	371	317
0.41	4.29 ± 0.36	270	261

[a]Values extracted from Caro *et al.*[4]

parameters. The measured biaxial elastic modulus and CTE could be beneficial for designing the next generation $Al_{1-x}Sc_xN$-based RF-MEMS, and the temperature-dependent CTE could be used in predicting device performance at elevated operating temperatures.

We gratefully acknowledge our colleagues S. Leone and S. Müller for the sapphire substrates, R. Iannucci for helping with EDX measurements, and T. Hugger for assistance with the laser profiler measurements. This work was supported by the FhG Internal Programs under Grant No. Attract 005-600636.

[1] M. Akiyama, T. Kamohara, K. Kano, A. Teshigahara, Y. Takeuchi, and N. Kawahara, Adv. Mater. **21**, 593 (2009).
[2] G. Wingqvist, F. Tasnádi, A. Žukauskaitė, J. Birch, H. Arwin, and L. Hultman, Appl. Phys. Lett. **97**, 112902 (2010).
[3] A. Žukauskaitė, E. Broitman, P. Sandström, L. Hultman, and J. Birch, Phys. Status Solidi A **212**, 666 (2015).
[4] M. A. Caro, S. Zhang, T. Riekkinen, M. Ylilammi, M. A. Moram, O. Lopez-Acevedo, J. Molarius, and T. Laurila, J. Phys. Condens. Matter **27**, 245901 (2015).
[5] N. Kurz, Y. Lu, L. Kirste, M. Reusch, A. Žukauskaitė, V. Lebedev, and O. Ambacher, Phys. Status Solidi **215**, 1700831 (2018).
[6] M. Reusch, S. Cherneva, Y. Lu, A. Žukauskaitė, L. Kirste, K. Holc, M. Datcheva, D. Stoychev, V. Lebedev, and O. Ambacher, Appl. Surf. Sci. **407**, 307 (2017).
[7] J. Menk, *Nanoindentation in Materials Science* (InTech, 2012).
[8] R. E. Sah, L. Kirste, M. Baeumler, P. Hiesinger, V. Cimalla, V. Lebedev, H. Baumann, and H.-E. Zschau, J. Vac. Sci. Technol., A **28**, 394 (2010).
[9] T.-C. Chen, W.-J. Lin, and D.-L. Chen, J. Appl. Phys. **96**, 3800 (2004).
[10] R. Knepper and S. P. Baker, Appl. Phys. Lett. **90**, 181908 (2007).
[11] T. F. Retajczyk and K. A. Sinha, Thin Solid Films **70**, 241 (1980).
[12] Y. Lu, M. Reusch, N. Kurz, A. Ding, T. Christoph, L. Kirste, V. Lebedev, and A. Žukauskaitė, Phys. Status Solidi A **215**, 1700559 (2018).
[13] P. M. Mayrhofer, C. Eisenmenger-Sittner, M. Stöger-Pollach, H. Euchner, A. Bittner, and U. Schmid, J. Appl. Phys. **115**, 193505 (2014).
[14] H. Fukuyama, H. Miyake, G. Nishio, S. Suzuki, and K. Hiramatsu, Jpn. J. Appl. Phys., Part 2 **55**, 05FL02 (2016).
[15] H. Takeuchi, M. Ohtsuka, and H. Fukuyama, Phys. Status Solidi B **252**, 1163 (2015).
[16] W. J. Liauh, S. Wu, J. L. Huang, D. F. Lii, Z. X. Lin, and W. K. Yeh, Surf. Coatings Technol. **308**, 101 (2016).
[17] A. Žukauskaitė, G. Wingqvist, J. Palisaitis, J. Jensen, P. O. A. Persson, R. Matloub, P. Muralt, Y. Kim, J. Birch, and L. Hultman, J. Appl. Phys. **111**, 093527 (2012).
[18] S. Fichtner, T. Reimer, S. Chemnitz, F. Lofink, and B. Wagner, APL Mater. **3**, 116102 (2015).
[19] S. Mertin, B. Heinz, O. Rattunde, G. Christmann, M. A. Dubois, S. Nicolay, and P. Muralt, Surf. Coatings Technol. **343**, 2 (2018).
[20] C. Höglund, J. Birch, B. Alling, J. Bareño, Z. Czigány, P. O. A. Persson, G. Wingqvist, A. Žukauskaitė, and L. Hultman, J. Appl. Phys. **107**, 123515 (2010).
[21] K. Lefki and G. J. M. Dormans, J. Appl. Phys. **76**, 1764 (1994).
[22] M. A. Hopcroft, W. D. Nix, and T. W. Kenny, J. Microelectromech. Syst. **19**, 229 (2010).
[23] G. G. Stoney, Proc. R. Soc. A **82**, 172 (1909).
[24] W. M. Yim and R. J. Paff, J. Appl. Phys. **45**, 1456 (1974).
[25] V. Pishchik, L. A. Lytvynov, and E. R. Dobrovinskaya, *Sapphire: Material, Manufacturing, Application* (Springer US, Boston, MA, 2009).
[26] Y. Kurokawa, K. Utsumi, H. Takamizawa, T. Kamata, and S. Noguchi, IEEE Trans. Compon., Hybrids, Manuf. Technol. **8**, 247 (1985).
[27] G. A. Slack and S. F. Bartram, J. Appl. Phys. **46**, 89 (1975).
[28] S. Zhang, W. Y. Fu, D. Holec, C. J. Humphreys, and M. a. Moram, J. Appl. Phys. **114**, 243516 (2013).
[29] C. M. Lin, T. T. Yen, Y. J. Lai, V. V Felmetsger, M. A. Hopcroft, J. H. Kuypers, and A. P. Pisano, IEEE Trans. Ultrason. Ferroelectr. Freq. Control **57**, 524 (2010).
[30] G. Wingqvist, L. Arapan, V. Yantchev, and I. Katardjiev, J. Micromech. Microeng. **19**, 035018 (2009).
[31] S. Figge, H. Kröncke, D. Hommel, and B. M. Epelbaum, Appl. Phys. Lett. **94**, 101915 (2009).